



HAL
open science

Simulations of initially highly disturbed jets with experiment-like exit boundary layers

Christophe Bogey, Olivier Marsden

► **To cite this version:**

Christophe Bogey, Olivier Marsden. Simulations of initially highly disturbed jets with experiment-like exit boundary layers. *AIAA Journal*, 2016, 54, pp.1299-1312. 10.2514/1.J054426 . hal-01516112

HAL Id: hal-01516112

<https://hal.science/hal-01516112>

Submitted on 30 Jun 2024

HAL is a multi-disciplinary open access archive for the deposit and dissemination of scientific research documents, whether they are published or not. The documents may come from teaching and research institutions in France or abroad, or from public or private research centers.

L'archive ouverte pluridisciplinaire **HAL**, est destinée au dépôt et à la diffusion de documents scientifiques de niveau recherche, publiés ou non, émanant des établissements d'enseignement et de recherche français ou étrangers, des laboratoires publics ou privés.

Simulations of Initially Highly Disturbed Jets with Experiment-Like Exit Boundary Layers

Christophe Bogey* and Olivier Marsden†
Université de Lyon, École Centrale de Lyon, 69134 Ecully, France

Two isothermal round jets at a Mach number of 0.9 and a diameter-based Reynolds number of 2×10^5 have been computed by compressible large-eddy simulation using high-order finite differences on a grid of 3.1 billion points. At the exit of a straight pipe nozzle in which a trip forcing is applied, the jet flow velocity parameters, including the momentum thickness and the shape factor of the boundary layer, the momentum-thickness-based Reynolds number, and the peak turbulence intensity, roughly match those found in experiments using two nozzles referred to as the ASME and the conical nozzles. The boundary layer is in a highly disturbed laminar state in the first case and in a turbulent state in the second. The exit flow conditions, the shear-layer and jet flowfields, and the far-field noise provided by the large-eddy simulation are described. The jet with the ASME-like initial conditions develops a little more rapidly, with slightly higher turbulence levels than the other. Overall, however, the results obtained for the two jets are very similar, and they are in good agreement with measurements available for Mach 0.9 jets. In particular, this similarity holds for the far-field spectra. Because the ASME nozzle has been reported to yield higher noise levels than the conical nozzle, this suggests that the nozzle-exit conditions in the large-eddy simulation do not adequately reflect those in the experiments and/or that the link between the noise differences and the jet initial conditions using the two nozzles is not as simple as was first thought, and that other parameters, associated for instance with the nozzle geometry such as the presence of pressure gradients, may also play an important role.

I. Introduction

SINCE the work of Crow and Champagne [1] in 1971, it has been well known that the aerodynamic and acoustic characteristics of free shear flows depend on their initial conditions. For subsonic jets, important parameters are the thickness and the shape of the velocity profile as well as the turbulence level at the nozzle exit. Their effects on the shear-layer and jet flowfields as well as the acoustic far field have been described in the 1970s and 1980s by many researchers, including Hill et al. [2], Browand and Latigo [3], Husain and Hussain [4], Raman et al. [5,6], Zaman [7,8], and Bridges and Hussain [9]. In particular, it has been established that initially laminar jets develop more rapidly and generate more noise than initially turbulent jets.

In simulations, the issue of the initial conditions is a crucial one; refer to the review papers by Colonius and Lele [10], Bailly and Bogey [11], Wang et al. [12], and Bodony and Lele [13]. In the computations carried out in the late 1990s and early 2000s, using direct numerical simulation, as in Boersma et al. [14], Stanley and Sarkar [15], and Freund [16], or large-eddy simulation (LES), as in Zhao et al. [17], Bogey et al. [18], and Bodony and Lele [19], the limited computational resources made it very difficult to prescribe jet initial conditions corresponding to measured conditions, notably in terms of shear-layer thickness [13]. The usual approach was therefore to specify a velocity profile at the inflow, onto which random disturbances or instability modes are added to seed the turbulence. It was the case in the three LES mentioned previously as well as in the

studies by Bogey and Bailly [20] and Kim and Choi [21] focusing on the sensitivity to jet initial conditions and forcing. Since then, other approaches have been developed. One possibility is to impose an inflow velocity profile provided by a steady-state computation inside the nozzle, as done in Shur et al. [22]. Another is to include the final part of the nozzle geometry (e.g., in Andersson et al. [23]) or a pipe nozzle in the computational domain. Following the latter strategy, LESs have been run over the past few years by Bogey et al. [24–29] for initially laminar and highly disturbed jets at a Mach number of $M = u_j/c_a = 0.9$ and Reynolds numbers $Re_D = u_j D/\nu_j$ between 25,000 and $Re_D = 200,000$, with laminar exit boundary-layer profiles, where D , u_j , c , and ν are the jet diameter and velocity, the speed of sound, and the kinematic molecular viscosity, and subscripts j and a denote inflow and ambient conditions. Attempts to compute initially turbulent jets have been made by Bogey et al. [30] and Uzun and Hussaini [31], using a coarse grid in the former case and a grid with a spatial extent limited to 4.5 diameters downstream of the nozzle in the latter. Subsequently, Sandberg et al. [32] performed the simulation of a fully turbulent pipe flow at $Re_D = 7500$ exiting into a coflow, and Bühler et al. [33] successfully computed a jet at $Re_D = 18,100$ with turbulent conditions at the exit of a pipe nozzle. LESs of jets at $Re_D = 50,000$ with thick transitional and turbulent boundary-layer profiles have been carried out in Bogey and Marsden [34]. Finally, Brès et al. [35] and Le Bras et al. [36] very recently simulated initially turbulent jets at $Re_D > 500,000$ using wall modeling inside the nozzle.

In experiments, the question of the initial conditions has received renewed attention since Viswanathan's claim [37] in 2004 that the jet noise database of Tanna [38] might be contaminated by spurious facility noise. In reply to this, Harper-Bourne [39] suggested that the extra components observed at high frequencies in Tanna's sound spectra [38] are due to laminar flow conditions at the nozzle exit. This seems to be confirmed by the experimental results acquired by Viswanathan and Clark [40], Zaman [41], and Karon and Ahuja [42] for jets exiting from the ASME and the conical nozzles of identical exit diameter, differing in internal profile. Indeed, less high-frequency noise is produced using the conical nozzle, which is the nozzle providing the most developed exit boundary layers (BLs), as indicated by the measurements by Zaman [41] and Karon and Ahuja [42] for jets over a wide range of Mach numbers. For illustrative purposes, the sound pressure levels (SPLs) obtained by the first author at the radiation angles of 60 and 90 deg for Mach 0.896 jets using nozzles of 1-in. exit diameter are presented in Figs. 1a and 1b. Compared to the

*Research Scientist CNRS, Laboratoire de Mécanique des Fluides et d'Acoustique, UMR CNRS 5509; christophe.bogey@ec-lyon.fr. Senior Member AIAA and Associate Fellow AIAA.

†Assistant Professor, Laboratoire de Mécanique des Fluides et d'Acoustique, UMR CNRS 5509; currently Research Scientist, Earth-System Assimilation Section, ECMWF, Shinfield Park, Reading RG29AX, U.K.; olivier.marsden@ec-lyon.fr.

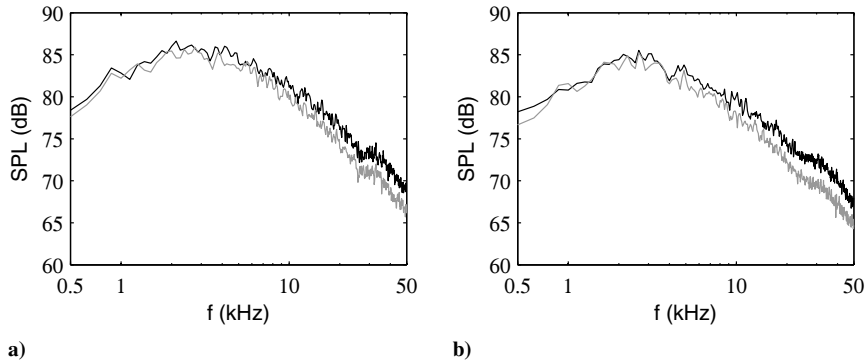


Fig. 1 SPLs obtained by Zaman [41] at a) 60 deg, and b) 90 deg, relative to the jet direction, for Mach 0.896 jets using ASME (black line) and conical (grey line) nozzles.

conical case, they are stronger by 2–3 dB in the ASME case at frequencies $f \geq 4$ kHz, that is at Strouhal numbers $St_D = fD/u_j \geq 0.3$. In a very recent work on the same topic, Fontaine et al. [43] also explored the shear-layer flow properties and the noise of three initially highly disturbed jets using nozzles of various lengths yielding different exit conditions. The jet with a partially developed exit boundary layer generates 3 dB more intense sound than the two others with fully turbulent boundary layers. This trend is in agreement with that observed with the ASME and the conical nozzles.

Coming back to the issue of the ASME and the conical nozzles, results obtained just downstream the nozzle by Zaman [41] for $M = 0.37$ and nozzles of 1 in. diameter and by Karon and Ahuja [42] for $M = 0.4$ and $D = 1.5$ in. are provided in Table 1. In all cases, the boundary layers are very thin relative to the jet radius $r_0 = D/2$, but they have a larger momentum thickness δ_θ , leading to a higher Reynolds number $Re_\theta = u_j \delta_\theta / \nu_j$, using the conical nozzle. More importantly, they are in a laminar state with the ASME nozzle but in a turbulent state with the conical nozzle. This is supported, in particular, by the shape factors of $H = \delta^*/\delta_\theta = 2.34$ and 1.71, where δ^* is the boundary-layer displacement thickness, reported by Karon and Ahuja [42] in the two cases. As for the peak axial turbulence intensities u'_e/u_j , where u'_e is the maximum rms value of axial velocity fluctuations near the nozzle exit, they have been found by Zaman [41] to be equal to 11.5% with the ASME nozzle and 7% with the conical nozzle. Thus, the laminar boundary layers from the ASME nozzle appear to be highly disturbed and to contain stronger velocity fluctuations than the turbulent boundary layers from the conical nozzle, which is counterintuitive and may result in some confusion. Moreover, little is known about the flowfields of the jets. For these reasons, it is interesting to investigate the properties of these jets using numerical simulations.

In the present work, two isothermal round jets have been calculated using LES on a grid containing 3.1 billion points using low-dissipation and low-dispersion finite differences and relaxation filtering as subgrid-scale dissipation. The jets have a Mach number $M = 0.9$ and a Reynolds number $Re_D = 2 \times 10^5$. They originate from a $2r_0$ -long straight pipe nozzle, at the inlet of which mean velocity profiles are imposed and in which a triplike forcing is employed [25] to generate a desired level of turbulent fluctuations at the exit. The inlet velocity profiles and the forcing position and strength have been chosen to obtain exit flow conditions, in terms of momentum thickness and the shape factor of the boundary layer,

momentum-thickness-based Reynolds number, and peak turbulence intensity, similar to those given in Table 1 for the ASME and the conical nozzles. Consequently, the nozzle-exit boundary layer is in a highly disturbed laminar state in the first jet and in a turbulent state in the second one. In this work, two objectives are pursued. The first one is to perform the LES of jets with experimentlike initial flow velocity parameters at a very high resolution and to compare the results with available experimental data for laboratory jets at a Mach number of 0.9. The second one is to examine the differences between the flow and acoustic fields of the two jets and to determine whether they correspond to those measured between the jets from the ASME and the conical nozzles.

The paper is organized as follows. The main characteristics of the different jets and of the simulations, including inflow conditions, numerical methods, and computational parameters, are documented in Sec. II. The nozzle-exit flow properties, the mixing-layer and jet flowfields, and the jet acoustic fields are described in Sec. III. Concluding remarks are given in Sec. IV. Finally, results from an additional simulation using a finer grid are depicted in the Appendix to demonstrate the accuracy of the LES of the jet with a turbulent exit boundary layer.

II. Parameters

A. Jet Definition

Two jets, referred to as jetASME and jetConic, are considered. They are isothermal and have a Mach number of $M = 0.9$ and a Reynolds number of $Re_D = 2 \times 10^5$. The ambient temperature and pressure are $T_a = 293$ K and $p_a = 10^5$ Pa. The jets originate at $z = 0$ from a pipe nozzle of radius r_0 and length $2r_0$, whose lip is $0.05r_0$ thick. At the pipe inlet, different axial velocity profiles are imposed. Radial and azimuthal velocities are set to zero, pressure is equal to p_a , and temperature is determined by a Crocco–Busemann relation. A triplike forcing is applied to the boundary layers in the pipe to generate disturbed exit conditions for the jets, which otherwise would initially contain only very weak velocity fluctuations. The main parameters of the pipe-inlet axial velocity profiles and of the boundary-layer excitations are collected in Table 2. They have been chosen to obtain exit boundary-layer conditions similar to those reported in Table 1 for the jets of Zaman [41] and Karon and Ahuja [42], as will be shown later in Sec. III.B.

The inlet axial velocity profiles are represented in Fig. 2a. In jetASME, the profile is a Blasius laminar boundary-layer profile with

Table 1 Jet initial conditions in experiments

Nozzle	D , in.	M	Re_D	BL state	H	δ_θ/r_0	Re_θ	u'_e/u_j , %
<i>Zaman [41]</i>								
ASME	1	0.37	2.2×10^5	Laminar	—	0.0050	556	11.5
Conical	1	0.37	2.2×10^5	Turbulent	—	0.0106	1179	7
<i>Karon and Ahuja [42]</i>								
ASME	1.5	0.40	3.5×10^5	—	2.34	0.0049	870	—
Conical	1.5	0.40	3.5×10^5	—	1.71	0.0065	1135	—

Table 2 Jet inflow parameters, and strength and position of the trip-like excitation

Jet	M	Re_D	H	δ_θ/r_0	δ_{99}/r_0	α_{trip}	z_{trip}
jetASME	0.9	2×10^5	2.55	0.0053	0.037	0.0395	$-0.125r_0$
jetConic	0.9	2×10^5	1.52	0.0117	0.104	0.0231	$-0.35r_0$

a shape factor $St_\theta = 0.013$, given by Pohlhausen's fourth-order polynomial approximation:

$$\frac{u_{\text{inlet}}(r)}{u_j} = \begin{cases} \frac{(r_0 - r)}{\delta_{\text{BL}}} \left[2 - 2 \left(\frac{r_0 - r}{\delta_{\text{BL}}} \right)^2 + \left(\frac{r_0 - r}{\delta_{\text{BL}}} \right)^3 \right] & \text{if } r \geq r_0 - \delta_{\text{BL}} \\ 1 & \text{otherwise} \end{cases} \quad (1)$$

with $\delta_{\text{BL}} = 0.0045r_0$, yielding a momentum thickness of $\delta_\theta = 0.0053r_0$ and a 99% velocity thickness of $\delta_{99} = 0.037r_0$. In jetConic, the inlet velocity profile is transitional boundary-layer profile [34] with $H = 1.52$ defined as

$$\frac{u_{\text{inlet}}(r)}{u_j} = \begin{cases} \left(\sin \left[\frac{\pi}{2} \left(\frac{r_0 - r}{\delta_{T_2}} \right)^{\beta_2} \right] \right)^{\gamma_2} & \text{if } r \geq r_0 - \delta_{T_2} \\ 1 & \text{otherwise} \end{cases} \quad (2)$$

where $\beta_2 = 0.423$, $\gamma_2 = 0.82$, and $\delta_{T_2} = 0.1328r_0$, leading to $\delta_\theta = 0.0117r_0$ and $\delta_{99} = 0.104r_0$. This profile was designed to fit the experimental data obtained by Schubauer and Klebanoff [44] in a flat-plate boundary layer in the region of changeover from laminar to fully turbulent conditions; refer to Appendix A of a recent paper [34].

The two jets are ‘‘tripped’’ using an arbitrary tripping device [45–50] whose parameters are determined by trial and error, as is usually done in laboratory experiments for boundary layers over a flat plate or in jet nozzles (e.g., in Klebanoff and Diehl [45] and Crow and Champagne [1]). In experiments, the trip devices can be of various kinds, such as rough strips, rings or round wires mounted at the wall, grids or screens in the flow, or pipe extensions. In simulations, transition to turbulence can, for instance, be induced by applying a volume force in the near-wall region or by imposing random fluctuations, synthetic turbulence, or instability modes on the flow profiles. In the present jets, the forcing procedure detailed in Appendix A of Bogey et al. [25] is implemented. It consists of adding random low-level vortical disturbances uncorrelated in the azimuthal direction in the boundary layers and has been previously applied to both laminar [25–29] and nonlaminar [34] velocity profiles. The position and the strength of the forcing are indicated in Table 2. They have been adjusted to reach peak turbulence intensities of about 11.5% in jetASME and 7% in jetConic at $z = 0.04r_0$ close to the nozzle exit, as in the jets of Zaman [41] considered in Table 1. This point is illustrated in Fig. 2b showing the variations of the maximum rms value of axial velocity fluctuations in the pipe and just downstream. On the

basis of previous studies and preliminary tests, the forcing is located at $z_{\text{trip}} = -0.125r_0$ in jetASME and $z_{\text{trip}} = -0.35r_0$ in jetConic, and the values of the coefficient α_{trip} specifying the forcing strength are set to 0.046 and 0.095, respectively. Finally, pressure fluctuations of maximum amplitude 200 Pa, random in both space and time, are added in the shear layers between $z = 0.25r_0$ and $z = 4r_0$ only at the very beginning of the simulations, from $t = 0$ up to nondimensional time $t = 12.5r_0/u_j$, to speed up the initial transient period.

B. Large-Eddy Simulation Procedure and Numerical Methods

The LES are carried out using a solver of the three-dimensional filtered compressible Navier–Stokes equations in cylindrical coordinates (r, θ, z) based on low-dissipation and low-dispersion explicit schemes. The axis singularity is taken into account by the method of Mohseni and Colonius [51]. To alleviate the time-step restriction due to the shrinking azimuthal mesh spacing near the cylindrical origin, the derivatives in the azimuthal direction around the axis are calculated at coarser resolutions than permitted by the grid [52]. For the points closest to the jet axis, the effective azimuthal discretization is thus equal to $2\pi/32$. Fourth-order 11-point centered finite differences are used for spatial discretization, and a second-order six-stage Runge–Kutta algorithm is implemented for time integration [53]. A 12th-order 13-point centered filter [54] is applied explicitly to the flow variables every time step. Noncentered finite differences and filters are also used near the pipe walls and the grid boundaries [24,55]. The radiation conditions of Tam and Dong [56] are applied at all boundaries, with the addition at the outflow of a sponge zone combining grid stretching and Laplacian filtering [57].

The explicit filtering is employed to remove grid-to-grid oscillations but also as a subgrid high-order dissipation model to relax turbulent energy from scales at wave numbers close to the grid cutoff wave number while leaving larger scales mostly unaffected [58–61]. To check this point, and to assess the reliability of the present LES, the transfer functions associated with molecular viscosity, relaxation filtering, and time integration are compared as proposed in Bogey et al. [25]. They are evaluated for the minimum and maximum mesh spacings in the jets, namely the radial mesh spacing at $r = r_0$ and the axial mesh spacing at $z \geq 25r_0$. They are presented in Figs. 3a and 3b as a function of the normalized wave number $k\Delta$, where Δ is the mesh spacing. For $\Delta = \Delta r(r = r_0)$, in Fig. 3a, the transfer function of molecular viscosity is found to be higher than that of the relaxation filtering for wave numbers $k\Delta < 1.52$, corresponding to wavelengths $\lambda/\Delta > 4.13$, and inversely lower for $k\Delta > 1.52$ and $\lambda/\Delta < 4.13$. A similar behavior is noticed in Fig. 3b for $\Delta = \Delta z(z \geq 25r_0)$. Here, the two dissipation functions intersect at $k\Delta = 0.49$, that is for $\lambda/\Delta = 12.72$ points per wavelength. In both figures, in addition, the transfer function of time integration is well below that of viscosity for all wave numbers. These results indicate that the largest turbulent structures in the LES are mainly dissipated by molecular viscosity. The physics of these structures is therefore unlikely to be governed by either numerical or subgrid-modeling dissipation. This should allow the effective flow Reynolds number not to be artificially decreased

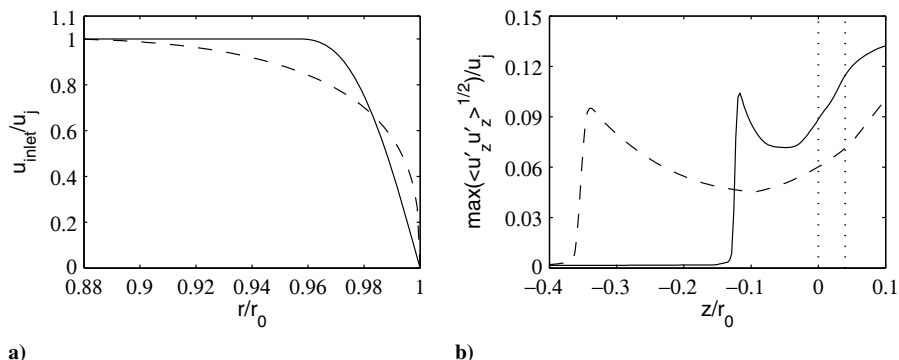


Fig. 2 Representations of a) the axial velocity profile u_{inlet} , and b) the peak rms value of u'_z : jetASME (solid line), jetConic (dashed line); $z = 0$ and $z = 0.04r_0$ (dotted line).

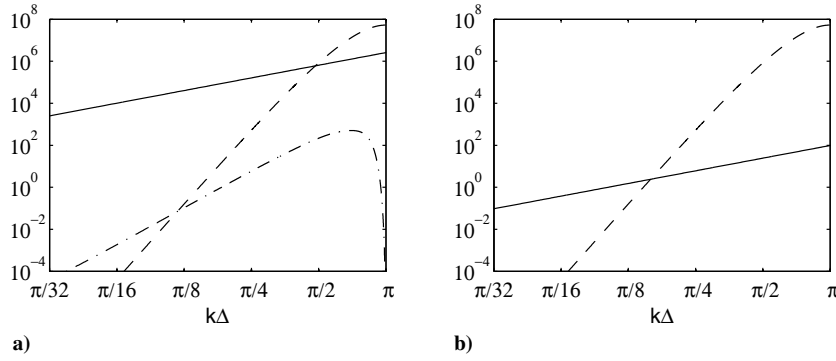


Fig. 3 Dissipation functions associated with molecular viscosity (solid line), filtering (dashed line), and time integration (dash-dotted line), as a function of $k\Delta$ for a) $0.0015r_0$, and b) $0.025r_0$.

and viscosity effects to be captured, as was the case in a previous study [28].

C. Simulation Parameters

As mentioned in Table 3, the LES grid contains $n_r \times n_\theta \times n_z = 496 \times 2048 \times 3052 = 3.1$ billion points. There are 393 points along the pipe nozzle between $z = -2r_0$ and $z = 0$ and 151 points between $r = 0$ and $r = r_0$. The physical domain extends axially down to $L_z = 28.4r_0$ and radially out to $L_r = 8.4r_0$.

The mesh spacings are uniform in the azimuthal direction, yielding $r\Delta\theta/r_0 = 0.31\%$ at $r = r_0$, but they vary in the radial and axial directions, as shown in Figs. 4a and 4b. In the radial direction, the mesh spacing is minimal at $r = r_0$, where $\Delta r/r_0 = 0.15\%$. On both sides of the nozzle lip line, it increases at a rate of 1.68% to reach $\Delta r/r_0 = 1.5\%$ at $r = 0$ on the jet axis and $\Delta r/r_0 = 5\%$ at $r = 3.9r_0$. Beyond $r = 3.9r_0$, the mesh spacing is constant up to $r = L_r = 8.4r_0$ and then grows again up to a value of $\Delta r/r_0 = 17.6\%$. This allows the radial boundary of the computational domain to be pushed back to $r = 14r_0$. In the axial direction, the mesh spacing is minimal between $z = -r_0$ and $z = 0$, where $\Delta z/r_0 = 0.31\%$. It increases upstream of $z = -r_0$ but also downstream of the nozzle exit at a rate of 0.087% up to $z = 25r_0$. The mesh spacing is thus equal to $\Delta z/r_0 = 2.5\%$ between $z = 25r_0$ and $z = L_z = 28.4r_0$. Further downstream, a 120-point sponge zone is applied using a grid stretching rate of 4.2%. Note that there are discontinuities in the mesh spacing slope. Because of their small number and to the low mesh stretching rates, they are, however, very unlikely to deteriorate the simulation accuracy significantly.

The LES grid has been built using 3.1 billion points, with attention paid to obtaining very fine discretization everywhere in the jet in the three spatial directions; see for instance the radial and axial mesh spacings provided in Table 3. The minimum mesh spacings of $\Delta r/r_0 = 0.15\%$, $r_0\Delta\theta/r_0 = 0.31\%$, and $\Delta z/r_0 = 0.31\%$ have specifically been chosen to compute the thin boundary layers and shear layers of the jets properly. These values have been set based on previous results obtained for Mach 0.9 jets using similar numerical methods and a grid with minimum mesh spacings of $\Delta r/r_0 = 0.36\%$, $r_0\Delta\theta/r_0 = 0.61\%$, and $\Delta z/r_0 = 0.72\%$, which are about two times larger than those in the present grid. In an early study, in particular, a jet with a laminar, highly disturbed boundary layer, characterized by $\delta_{BL} = 0.09r_0$ at the pipe-nozzle inlet and $Re_\theta = 487$ and $u'_e/u_j = 9.13\%$ at the exit, was simulated. The flow properties downstream of the nozzle were found to be independent of the grid [29]. Consequently, the grid resolution can be expected to be

appropriate in the jetASME case exhibiting a laminar inlet boundary-layer profile with $\delta_{BL} = 0.045r_0$, and $Re_\theta = 580$ and $u'_e/u_j = 8.86\%$ at the nozzle exit, as will be reported in Sec. III.B.

Regarding the jetConic case with an inlet transitional boundary-layer profile of thickness $\delta_{T_2} = 0.1328r_0$ and exit parameters of $Re_\theta = 1100$ and $u'_e/u_j = 6.02\%$ (see also in Sec. III.B), it can first be noted that a jet with $\delta_{T_2} = 0.332r_0$, $Re_\theta = 691$, and $u'_e/u_j = 6.14\%$ was recently calculated successfully on the grid mentioned previously [34]. In jetConic, the near-wall mesh spacings in the pipe expressed in wall units based on the wall friction velocity at the nozzle exit, given in Table 4, are equal to $\Delta r^+ = 3.7$, $(r_0\Delta\theta)^+ = 7.4$, and $\Delta z^+ = 7.4$. The azimuthal and axial mesh spacings are therefore sufficient because they meet the requirements needed to compute turbulent wall-bounded flows accurately, using direct numerical simulation as in Kim et al. [62] and Spalart [63] for instance, or using LES involving relaxation filtering as in Gloerfelt and Berland [64] and Kremer and Bogey [61]. For the wall-normal spacing, an additional LES has been performed using a finer grid. For $z \leq 3.5r_0$, this grid is identical to the first grid in the directions θ and z but differs in the radial direction with $\Delta r/r_0 = 0.08\%$ instead of $\Delta r/r_0 = 0.15\%$ at $r = r_0$. In the new LES, moreover, the tripping procedure is exactly the same as in the first LES, and the time step is halved because of the CFL stability condition, leading to an application of the relaxation filtering that is twice as frequent. The flowfields obtained using the two grids at the nozzle exit and in the mixing layers developing farther downstream have very similar features, as illustrated in the appendix. This demonstrates that the LES solutions do not depend significantly on the radial mesh spacing at $r = r_0$ or on the relaxation filtering.

The LES have run on 1024 processors of a distributed memory cluster using a hybrid message passing interface (MPI)–open multiprocessing (OpenMP) in-house solver and consumed about 2 million CPU hours. A total simulation time of $320r_0/u_j$ has been obtained for each jet, corresponding to 271,300 iterations in each case. After the initial transient period, density, velocity components, and pressure are recorded from time $t = 94r_0/u_j$ onward, on the jet axis and on two surfaces at $r = r_0$ and $r = r_c = 7.5r_0$, at a sampling frequency allowing the computation of spectra up to a Strouhal number $St_D = 20$. The cylindrical surface surrounding the jets is located at $r = 7.5r_0$, in a region where the radial mesh spacing yields a Strouhal number $St_D = 11.1$ for an acoustic wave discretized by four points per wavelength. In the azimuthal direction, every second grid point is stored, allowing data postprocessing to be performed up to the azimuthal mode $n_\theta = 1024$, where n_θ is the dimensionless azimuthal wave number such that $n_\theta = k_\theta r$. The

Table 3 Grid parameters: numbers of points, physical extents, and mesh spacings

Jet		$\Delta r/r_0$ (%) at $r =$				$\Delta z/r_0$ (%) at $z =$						
n_r	n_θ	n_z	L_r	L_z	0	r_0	$2r_0$	$4r_0$	0	$5r_0$	$15r_0$	$25r_0$
487	2048	3052	$8.4r_0$	$28.4r_0$	1.54	0.15	1.83	5	0.31	0.74	1.62	2.5

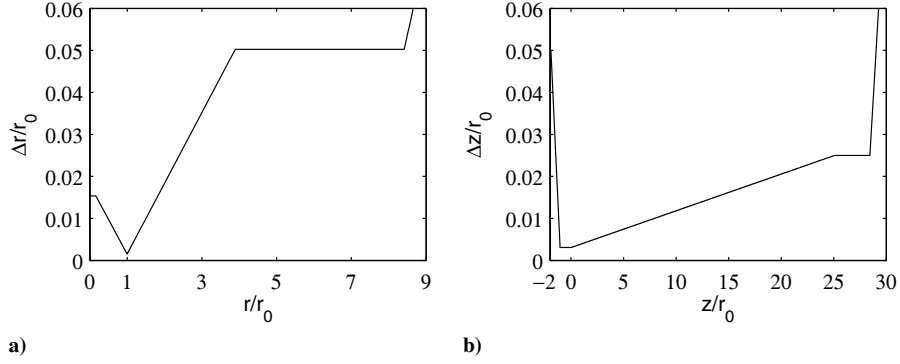


Fig. 4 Representation of the radial and axial mesh spacings: a) $\Delta r/r_0$, and b) $\Delta z/r_0$.

velocity spectra are evaluated from overlapping samples of duration $27.4r_0/u_j$. The flow statistics are determined from $t = 175r_0/u_j$ onward, and they are averaged in the azimuthal direction. They can be considered to be well converged in view of the results obtained at intermediary stages of the LES for $t \geq 300r_0/u_j$.

D. Far-Field Extrapolation

The near fields of jetASME and jetConic, obtained in the LES between $z = -2r_0$ and $z = L_z = 28.4r_0$ on the surface at $r = r_c = 7.5r_0$ mentioned previously, have been propagated to the acoustic far field. These calculations are performed from the isentropic linearized Euler equations (ILEEs) in cylindrical coordinates [65], using the same numerical methods as in the LES, and a grid containing $n_r \times n_\theta \times n_z = 2090 \times 512 \times 2000 = 2.3$ billion points. The grid extends axially from $z = -34r_0$ up to $z = 94r_0$ and radially from $r = r_c$ up to $r = 122r_0$. For $z \geq -2r_0$, the radial and axial mesh spacings are uniform with $\Delta r = \Delta z = 0.05r_0$, yielding $St_D = 11$ for an acoustic wave at four points per wavelength. The ILEEs are solved at the inner radial boundary using noncentered finite differences, except for the first row of points between $z = -2r_0$ and $z = L_z$, onto which the LES fluctuating velocities and pressure are imposed. Radiation conditions [56,57] are implemented at the outer radial boundary and at the inflow and outflow axial boundaries. After a time $t \simeq 120r_0/u_j$, pressure is recorded at a distance of $120r_0$ from $z = r = 0$, where far-field acoustic conditions are expected to apply according to experiments [66,67], for angles relative to the jet direction between $\varphi = 40$ deg and $\varphi = 90$ deg, during a period of about $200r_0/u_j$. Pressure spectra are evaluated using overlapping samples of duration $38r_0/u_j$, and they are averaged in the azimuthal direction.

III. Results

A. Vorticity and Pressure Snapshots

Snapshots of the vorticity norm obtained in the vicinity of the nozzle exit between $z = -0.4r_0$ and $z = 1.2r_0$, and in the shear layers up to $z = 15r_0$, are represented in Figs. 5a and 5b, Figs. 6a and 6b, respectively. In the first figures, the boundary-layer tripping due to the forcing at $z_{\text{trip}} = -0.125r_0$ in jetASME and $z_{\text{trip}} = -0.35r_0$ in jetConic is clearly visible. High levels of vorticity are found immediately downstream of the nozzle very near the lip line. As expected given the inlet boundary-layer thicknesses, they spread over a larger radial extent in jetConic than in jetASME. The region of changeover from boundary-layer to mixing-layer flow conditions also appears to be longer in the axial direction in jetConic. In that jet, the shear layer

shows turbulent structures elongated in the streamwise direction, typical of wall-bounded flows, close to the nozzle, then it rolls up around $z = 0.4r_0$ and is visually fully developed for about $z \geq r_0$. Farther downstream, in Figs. 6a and 6b, the mixing layers look quite similar in the two cases and exhibit large-scale structures resembling the coherent structures revealed by the flow visualizations of Brown and Roshko [68].

Snapshots of the vorticity norm and of the pressure field obtained down to $z = 28r_0$ simultaneously inside and outside the jets by LES are provided in Figs. 7a and 7b. The results in the two cases do not seem to be fundamentally different from each other. Both jets indeed exhibit a potential core ending around $z = 16r_0$ and large-scale near-field pressure fluctuations. The latter are classically associated with the flow coherent structures and have been discussed in Arndt et al. [69] and Coiffet et al. [70], for instance.

Finally, snapshots of the pressure fields computed up to a distance of $120r_0$ to the nozzle exit from the LES data at $r = 7.5r_0$ by solving the isentropic linearized Euler equations are displayed in Figs. 8a and 8b. For both jets, low-frequency acoustic components characterized by wavelengths $\lambda \simeq 15r_0$, yielding Strouhal numbers $St_D \simeq 0.15$, are dominant for small angles relative to the flow direction, which does not seem to be the case in the sideline direction. This is in agreement with the experimental observations of Mollo-Christensen et al. [71], Lush [72], and Tam et al. [73], among others. Acoustic waves at very low Strouhal numbers are also noted, especially in the jetASME case. On the basis of results obtained in a previous study [24] using two extrapolation surfaces at $r = 5.25r_0$ and at $r = 7.25r_0$ for an initially laminar jet, they are most likely to be spurious waves caused by the presence of aerodynamic fluctuations at the end of the LES surface used for the far-field wave extrapolations. Fortunately, they do not appear to affect the far-field spectra at Strouhal numbers $St_D \geq 0.1$ for radiation angles $\varphi \leq 75$ deg with respect to the jet axis, as will be shown in Sec. III.E.

B. Nozzle-Exit Conditions

The profiles of mean and rms axial velocities calculated at the nozzle exit of jetASME and jetConic are presented in Figs. 9a and 9b, and the main exit flow parameters are provided in Table 5. As intended, the exit boundary-layer profiles differ significantly in Fig. 9a. Their shape factors are equal to $H = 2.44$ and 1.88 ; their momentum thicknesses are $\delta_\theta = 0.0058r_0$ and $0.0111r_0$, yielding $Re_\theta = 580$ and 1110 ; and their 99% velocity thicknesses are $\delta_{99} = 0.041r_0$ and $0.102r_0$. The values of H , δ_θ/r_0 , and Re_θ in jetASME and jetConic are in line with the measurements of Zaman [41] and Karon and Ahuja [42] for jets from the ASME and the conical nozzles, respectively, in Table 1. The boundary-layer profile in the first jet corresponds to a laminar profile, and given that $H \simeq 1.45$ is obtained [47,48,63,74] for fully developed boundary layers at $Re_\theta \simeq 1000$, the profile in the second jet is transitional. As for the radial distributions of the rms values of velocity fluctuations in Fig. 9b, they also vary and reach peak values u'_e/u_j of 8.86% at $r_e = 0.992r_0$ in jetASME and of 6.02% at $r_e = 0.985r_0$ in jetConic. Therefore, the jet with a laminar exit velocity profile is initially more disturbed than the jet with a nonlaminar profile, which seems

Table 4 Near-wall mesh spacings in wall units at the nozzle exit

Jet	Δr^+	$(r_0 \Delta \theta)^+$	Δz^+
jetASME	3.0	6.0	6.0
jetConic	3.7	7.4	7.4

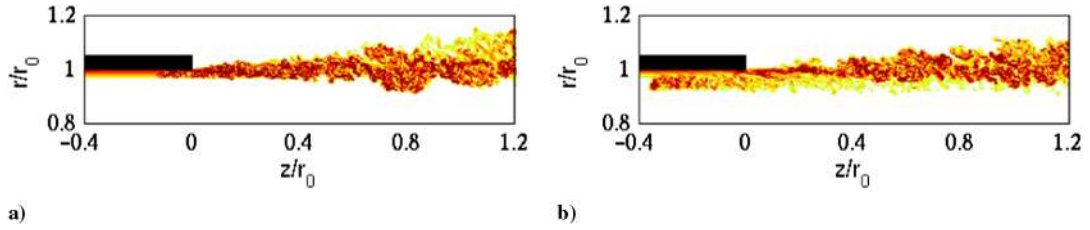


Fig. 5 Snapshots of vorticity norm for a) jetASME, and b) jetConic. The scale ranges up to the level of $48u_j/r_0$.

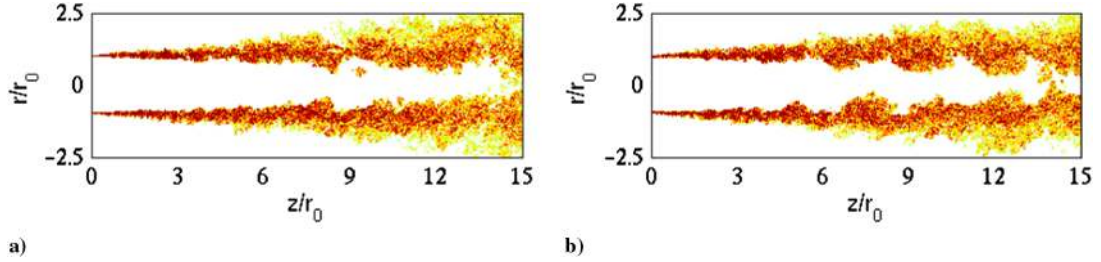


Fig. 6 Snapshots of vorticity norm for a) jetASME, and b) jetConic. The scale ranges up to the level of $14u_j/r_0$.

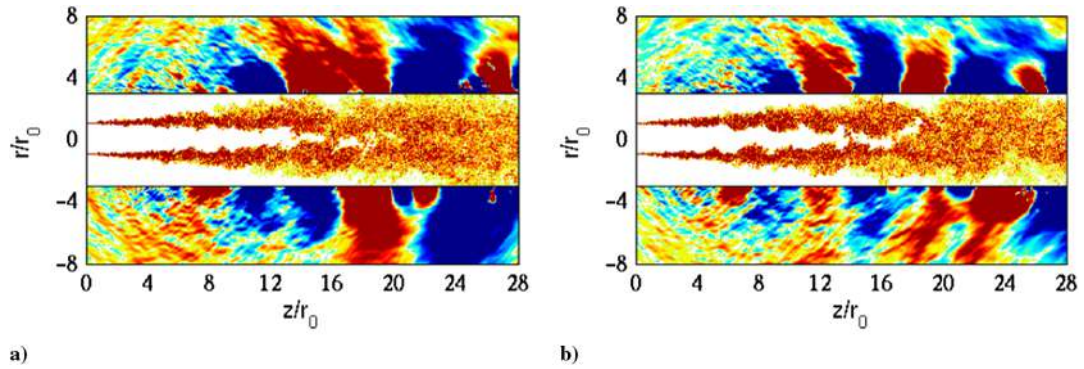


Fig. 7 Snapshots of vorticity norm and of pressure fluctuations for a) jetASME, and b) jetConic. The scales range up to the level of $8u_j/r_0$ for vorticity, and from -80 to 80 Pa for pressure.

contradictory but happens sometimes, as pointed out by Raman et al. [5].

The power spectral densities (PSD) of axial velocity fluctuations are evaluated at the nozzle exit at the position $r = r_e$ of the turbulence

intensity peak. They are represented as a function of the Strouhal number St_D in Fig. 10a and of the azimuthal mode n_θ in Fig. 10b. The levels are higher in the spectra of jetASME than in jetConic, which is not surprising in view of the maximum rms values u'_e/u_j in the two

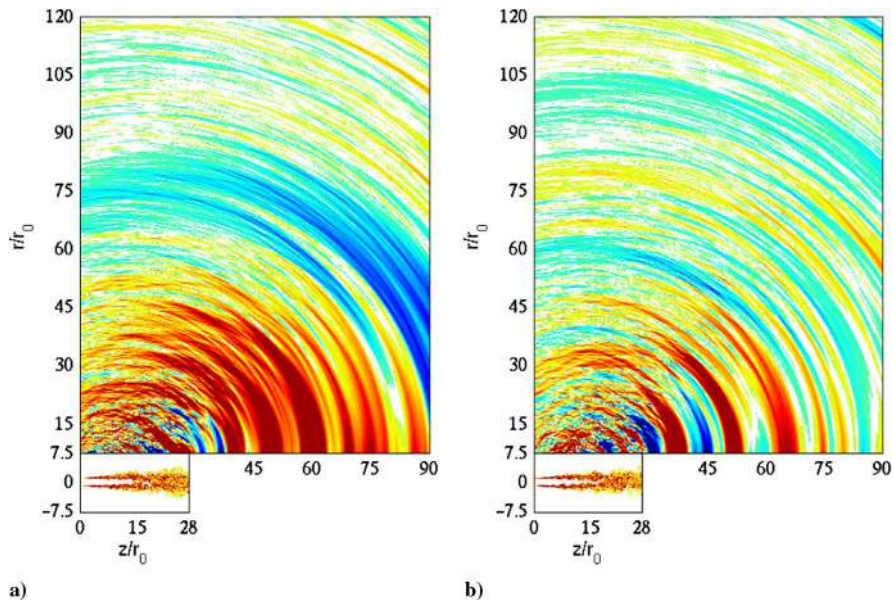


Fig. 8 Snapshots of vorticity norm and of pressure fluctuations for a) jetASME, and b) jetConic. The scales range up to the level of $8u_j/r_0$ for vorticity, and from -28 to 28 Pa for pressure.

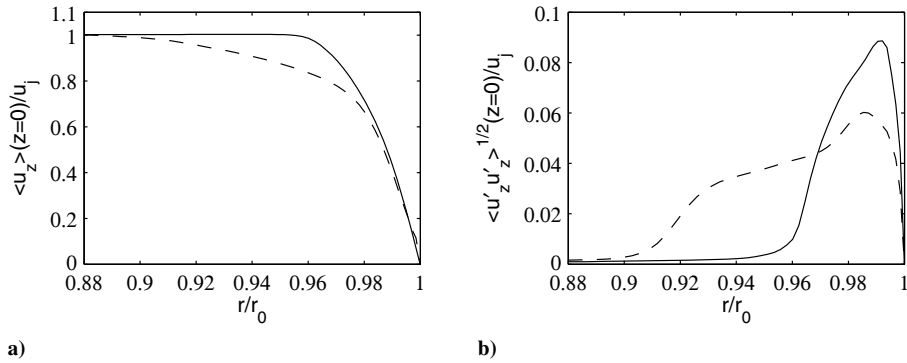


Fig. 9 Radial profiles at the nozzle exit of a) mean axial velocity $\langle u_z \rangle$, and b) the rms values of axial velocity fluctuations u'_z : jetASME (solid line), and jetConic (dashed line).

jets. The shapes of the spectra are roughly the same in the two cases and correspond, as was discussed in a note [26] on that matter, to the spectral shapes encountered for turbulent wall-bounded flows because of the presence of large-scale elongated structures [75]. The relative magnitude of the high-frequency components appears, however, stronger in the spectra of JetASME with a thinner boundary layer. The flat region observed for low Strouhal numbers in Fig. 10a thus extends up to $St_D \simeq 2.5$ in jetConic but to $St_D \simeq 5$ in jetASME. The dominant components in Fig. 10b also shift toward higher modes, resulting in peaks at $n_\theta^{\text{peak}} = 135$ in jetConic and at $n_\theta^{\text{peak}} = 203$ in jetASME, as reported in Table 5. At the location of peak turbulence level, the turbulent structures are consequently spaced out by $\lambda_\theta = 0.047r_0$ and $\lambda_\theta = 0.031r_0$, respectively. They are well discretized by the grid using mesh spacings of $0.0031r_0$ at $r = r_0$ in the azimuthal direction.

C. Shear-Layer Development

The variations over $0 \leq z \leq 15r_0$ of the momentum thickness δ_θ and of the spreading rate $d\delta_\theta/dz$ of the mixing layers are presented in Figs. 11a and 11b. In Fig. 11a, the shear-layer developments in the two jets turn out not to be significantly different and to agree fairly well with that measured by Fleury et al. [76] and Castelain [77] in isothermal, Mach 0.9 jets at $Re_D = 7.7 \times 10^5$ and $Re_D = 10^6$. It is a little faster in jetASME than in jetConic, leading to slightly higher values of spreading rates in Fig. 11b for the former jet. The curves in that figure both exhibit a double-hump shape, which is also noted in the experimental results obtained by Husain and Hussain [4] for an initially turbulent axisymmetric mixing layer at $30 \text{ m} \cdot \text{s}^{-1}$. They first grow rapidly with the axial distance just downstream of the nozzle to reach peak values of 0.27 at $z = 0.1r_0$ in jetASME and of 0.26 at $z = 0.4r_0$ in jetConic, and then decrease by about 20%. For $z \geq 1.5r_0$, they increase again, but more slowly than previously, up to $z = 10.2r_0$ in jetASME and to $z = 12r_0$ in jetConic, where they achieve values of around 0.27. Farther downstream, the spreading rates diminish as the end of the potential core is approached.

The peak rms values of axial and radial velocity fluctuations estimated between $z = 0$ and $z = 15r_0$ are displayed in Figs. 12a and 12b. Their streamwise evolutions in the two jets are very similar, showing a rapid growth downstream of the nozzle, a small hump near $z = r_0$, and then a very slow increase nearly up to $z = 15r_0$. They agree well with the experimental data obtained by Fleury [78] and Castelain [77] for Mach 0.9 jets using particle image velocimetry (PIV) and by Husain and Hussain [4] for an initially turbulent mixing layer at $30 \text{ m} \cdot \text{s}^{-1}$. The discrepancy in Fig. 12b with respect to

Fleury's data [78] is probably due to an underestimation of the turbulence values by the PIV method, which occurred in other jet experiments according to Bridges and Wernet [79]. The rms levels of velocity fluctuations are slightly higher in jetASME than in jetConic. A similar trend can be identified in Bogey and Marsden [34] and in Fontaine et al. [43]. In these studies, the turbulence intensities in the shear layers of initially highly disturbed jets are indeed stronger for a transitional nozzle-exit boundary-layer profile than for fully turbulent profiles. In the present jets, at $z = 6r_0$ for instance, the rms velocity levels are equal to 16.4 and 15.9% for u'_z , and of 11.5 and 11.1% for u'_r , respectively. The maximum levels, provided in Table 6, are however almost identical in the two jets. In particular, a peak value of 16.8% is found for the axial velocity fluctuations in both cases. This value is comparable to those measured by Husain and Hussain [4] in the similarity region of initially turbulent mixing layers.

The spectra of radial velocity fluctuations calculated on the lip line at the two axial locations $z = 0.2r_0$ and $z = 6r_0$ are presented in Figs. 13a and 13b as a function of the Strouhal number St_D . At the first location very near the nozzle, in Fig. 13a, an instabilitylike component appears to emerge in both jets. This component is centered around $St_D = 4.5$ in jetASME and $St_D = 4.8$ in jetConic, yielding Strouhal numbers based on the nozzle-exit momentum thickness of $St_\theta = 0.013$ and $St_\theta = 0.027$ as reported in Table 6. Therefore, the peak frequency obtained in jetASME with a laminar boundary-layer profile falls within the range of frequencies predominating early on in initially laminar mixing layers according to linear stability analyses [80] and experiments [81]. For jetConic with a transitional profile, it moves out of this range. The same tendency was observed for jets with thicker boundary-layer profiles in Bogey and Marsden [34]. In particular, a peak frequency at $St_\theta = 0.026$ was initially found in a jet with a nozzle-inlet profile given by Eq. (2) as in jetConic. Farther downstream at $z = 6r_0$, in Fig. 13b, the radial velocity spectra in the two jets display very similar broadband shapes and amplitudes over the whole range of frequencies considered.

D. Jet Development

The variations of the centerline mean axial velocity and of the jet half-width $\delta_{0.5}$, given by the radial position at which the mean velocity is equal to half of its centerline value, are presented in Figs. 14a and 14b. The curves obtained for the two jets are nearly superimposed but also reveal that the development of jetASME is slightly more rapid than that of jetConic, which is consistent with the differences in shear-layer spreading rate noted in the previous section. This leads to potential cores ending respectively at $z_c = 15.3r_0$ and $z_c = 15.6r_0$, as indicated in Table 7, with z_c being defined as the axial distance at which the centerline mean velocity is equal to $0.95u_j$. Furthermore, the LES profiles compare well with the experimental data available for four jets at a Mach number of 0.9 and Reynolds numbers $Re_D \geq 5 \times 10^5$, namely the cold jet of Bridges [82], the isothermal jets of Lau et al. [83] and Fleury et al. [76], and the slightly heated jet

Table 5 Nozzle-exit flow parameters

Jet	H	δ_0/r_0	δ_{99}/r_0	Re_θ	$u'_e/u_j, \%$	r_e/r_0	n_θ^{peak}
jetASME	2.44	0.0058	0.041	580	8.86	0.992	203
jetConic	1.88	0.0111	0.102	1110	6.02	0.985	135

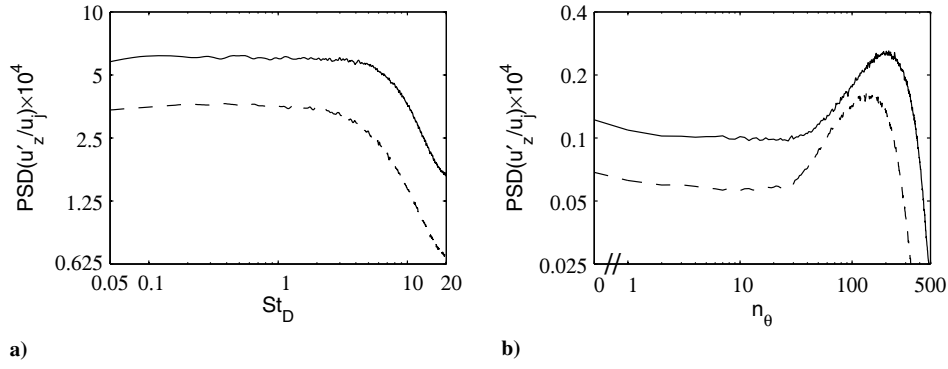


Fig. 10 PSDs of u'_z obtained at the nozzle exit at $r = r_e$, as functions of a) Strouhal number St_D , and b) azimuthal mode n_θ : jetASME (solid line), and jetConic (dashed line).

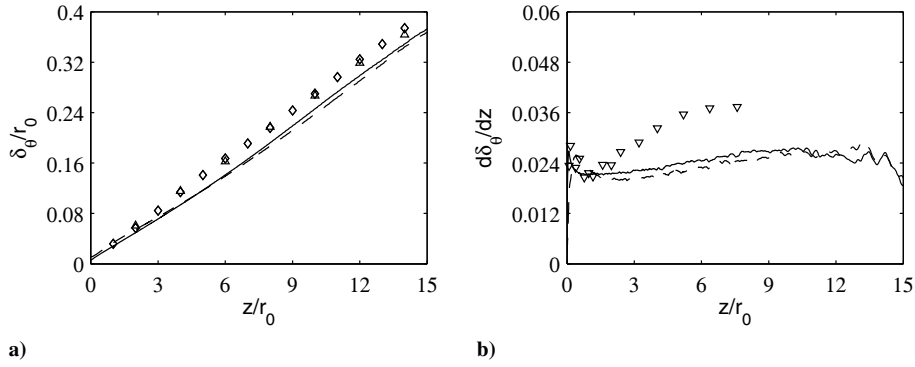


Fig. 11 Variations of a) momentum thickness δ_θ , and b) spreading rate $d\delta_\theta/dz$: jetASME (solid line), and jetConic (dashed line); measurements: \diamond Fleury [76], Δ Castelain [77], and ∇ Husain and Hussain [4].

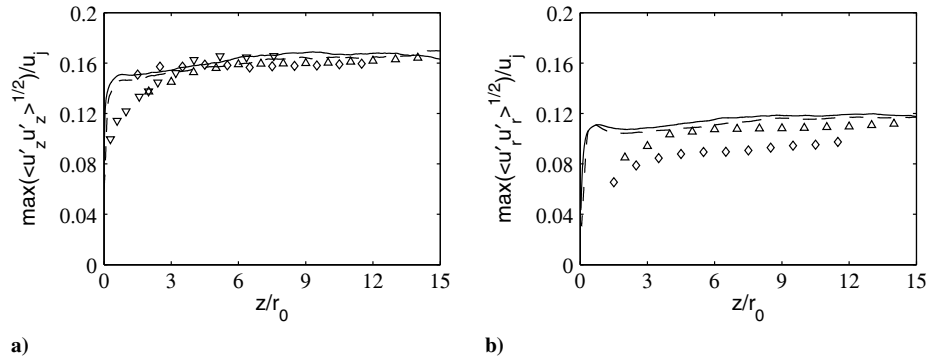


Fig. 12 Variations of the peak rms values of a) u'_z and b) u'_r : jetASME (solid line), jetConic (dashed line); measurements: \diamond Fleury [78], Δ Castelain [77], and ∇ Husain and Hussain [4].

of Arakeri et al. [84]. More precisely, they lie in the middle of the measurement points in Fig. 14a and pass through the points of Fleury et al. [76] in Fig. 14b.

The variations of the centerline rms values of axial and radial velocity fluctuations are shown in Figs. 15a and 15b. As is the case for the mean flow profiles, the results are very similar in jetASME and jetConic. In both jets, the peak turbulence intensities are reached around $z = 21r_0$ and are equal to about 15% for velocity u'_z and

11.5% for velocity u'_r ; see in Table 7 for the exact values. Compared to the experiments on Mach 0.9 jets mentioned previously, there is a good agreement with the data of Lau et al. [83] and Bridges [82]. The fluctuation levels obtained by Fleury et al. [76] and especially by Arakeri et al. [84] by performing PIV measurements are significantly lower. As pointed out in Sec. II.C after having seen the discrepancies in maximum radial turbulence intensities in Fig. 12b, this seems to be a frequent issue when the PIV technique is applied to jet flows [79].

Table 6 Peak turbulence intensities, and peak Strouhal numbers at $z = 0.2r_0$ and $r = r_0$

Jet	$\langle u'^2_z \rangle^{1/2} / u_j, \%$	$\langle u'^2_r \rangle^{1/2} / u_j, \%$	$\langle u'^2_\theta \rangle^{1/2} / u_j, \%$	$\langle u'_r u'_z \rangle^{1/2} / u_j, \%$	St_D	St_θ
jetASME	16.8	11.9	13.8	9.6	4.5	0.013
jetConic	16.8	12	13.6	9.4	4.8	0.027

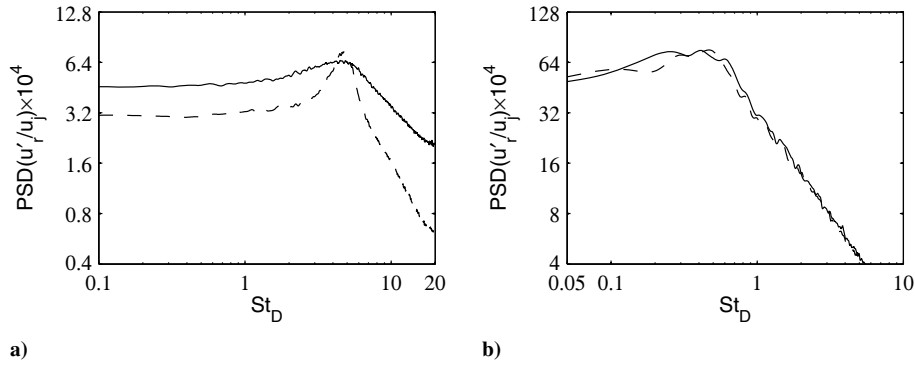


Fig. 13 PSDs of radial velocity fluctuations u'_r , a) at $z = 0.2r_0$ and $r = r_0$, and b) at $z = 6r_0$ and $r = r_0$, as functions of St_D : jetASME (solid line), and jetConic (dashed line).

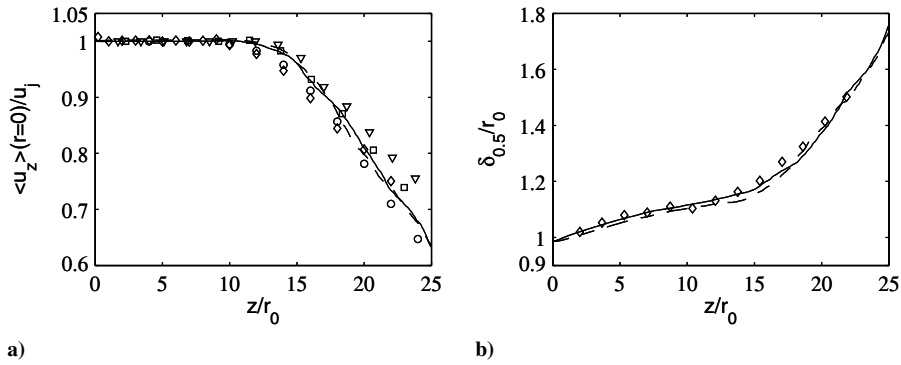


Fig. 14 Variations of a) mean axial on the jet axis, and b) jet half-width: jetASME (solid line), jetConic (dashed line); measurements: \circ Lau et al. [83], ∇ Bridges [82], \diamond Fleury et al. [76].

For completeness, the spectra of axial velocity fluctuations calculated at $z = 15.5r_0$, that is close to the end of the potential core in both jets, on the jet axis and on the nozzle lip line, are presented in Figs. 16a and 16b as a function of the Strouhal number St_D . The spectra at $r = 0$ are less smooth than those at $r = 0.5r_0$ because, unlike the latter, they cannot be averaged in the azimuthal direction. Despite this, the spectra obtained in jetASME and jetConic do not appear to differ much over the entire frequency range. They also strongly resemble the experimental spectra presented in Bridges and Wernet [85] for a cold, 51-mm-diam jet at a Mach number of 0.9.

E. Acoustic Fields

Far-field spectra determined for jetASME and jetConic from the pressure signals obtained at 120 radii from the nozzle exit from the LES near field by solving the isentropic linearized Euler equations are now displayed. The spectra computed at the radiation angles of $\varphi = 40, 60, 75,$ and 90 deg relative to the jet direction are represented in Figs. 17a–17d as a function of the Strouhal number St_D .

It appears that, for all angles and frequencies, the noise levels from jetASME and jetConic are very close. In addition, they agree very well with the spectra acquired by Bridges and Brown [86,87] for an

isothermal jet at $M = 0.9$ and $Re_D = 10^6$ at 150 radii from the nozzle exit, scaled to the distance of 120 radii. This experimental data set was chosen, among many others, because it has been proved not to be contaminated by extra sound sources, which could result from laminar upstream flow conditions, for example. Note in Fig. 17d that the spectra obtained for the present jets at $\varphi = 90$ deg are dominated by spurious components for $St_D \leq 0.2$, as mentioned in Sec. III.A and illustrated in Fig. 8a. However, as for the spectra at $\varphi = 40, 60,$ and 75 deg, they are nearly superimposed and fit the measurements of Bridges and Brown [86,87] for $St_D \geq 0.2$.

Given that the differences in turbulence intensities between the two jets are small both in the shear layers and on the jet axis in Figs. 12 and 14, it is not surprising that the jets generate similar noise levels. In particular, the jetASME simulation does not reproduce the noise increase observed for Strouhal numbers $St_D \geq 0.3$ in the experiments of Viswanathan and Clark [40], Zaman [41], and Karon and Ahuja [42] with the ASME nozzle, which is represented in Figs. 1a and 1b for the radiation angles $\varphi = 60$ and 90 deg. The reasons for this are for the moment unclear. One possibility is that the nozzle-exit conditions in the LES, and particularly in jetASME, do not correspond satisfactorily to the jet initial conditions in the experiments. One can wonder especially whether the use of a straight pipe nozzle instead of the full nozzle geometry is not an oversimplification and whether the jets with laminar boundary layers from the ASME nozzle really contain about 10% of rms velocity fluctuations at the nozzle exit. Another possibility, which does not exclude the first, is that the discrepancies in high-frequency noise between the ASME and the conical nozzles do not only result from the laminar and turbulent states of the exit boundary layers, but that other parameters, associated with the nozzle internal geometry for instance, also play an important role. Notably, as pointed out by Zaman [41], the nozzle geometry causes axial pressure gradients in the exit region, whose

Table 7 Length of the potential core and peak turbulence intensities on the centerline

Jet	z_c/r_0	$\langle u_z'^2 \rangle^{1/2}/u_j, \%$	$\langle u_r'^2 \rangle^{1/2}/u_j, \%$
jetASME	15.3	15	11.6
jetConic	15.6	14.8	11.2

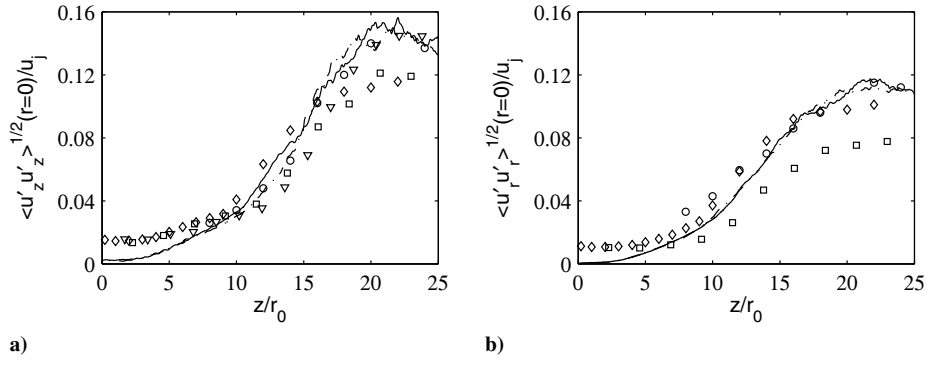


Fig. 15 Variations of the centerline rms values of a) u'_z and b) u'_r : jetASME (solid line), jetConic (dashed line); measurements: \circ Lau et al. [83], Arakeri et al. [84], ∇ Bridges [82], \diamond Fleury et al. [76].

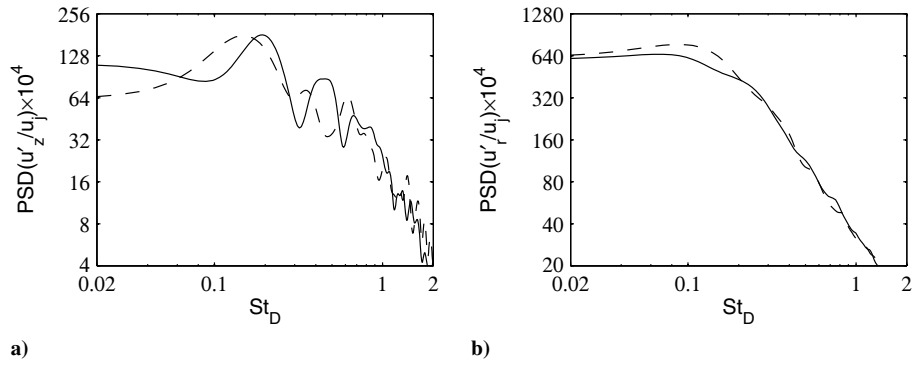


Fig. 16 PSDs of axial velocity fluctuations u'_z a) at $z = 15.5r_0$ and $r = 0$, and b) at $z = 15.5r_0$ and $r = r_0$, as functions of St_D : jetASME (solid line), and jetConic (dashed line).

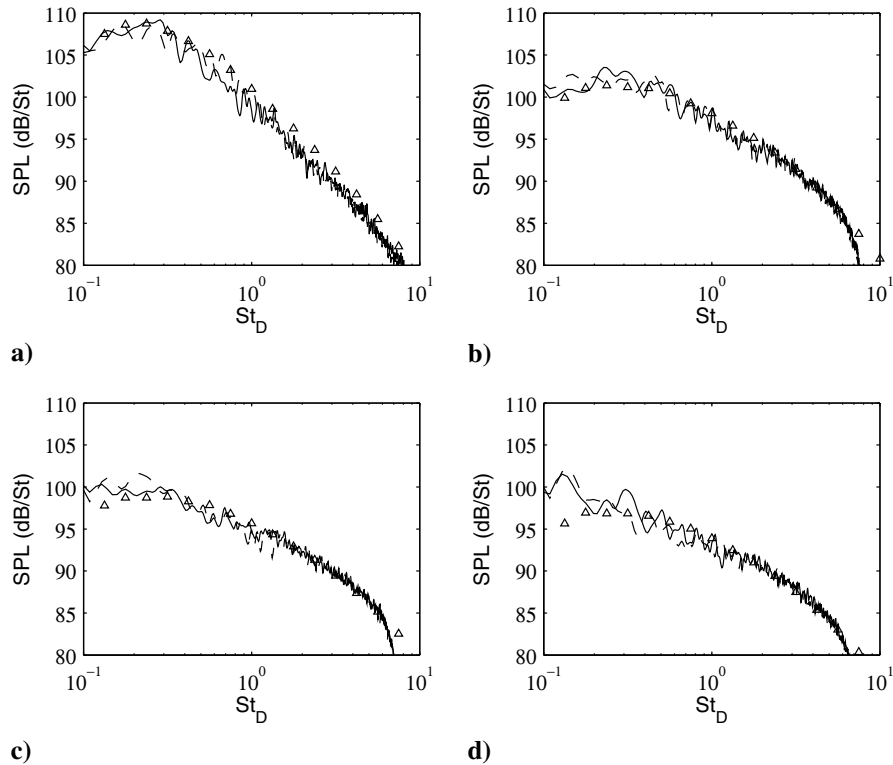


Fig. 17 SPLs obtained at $120r_0$ from the nozzle exit for a) 40 deg, b) 60 deg, c) 75 deg, and d) 90 deg, relative to the jet direction, as a function of St_D : jetASME (solid line), jetConic (dashed line); Δ measurements of Bridges and Brown [86,87].

effects on jet flow development and noise generation may need to be investigated.

IV. Conclusions

Two isothermal round jets at a Mach number of $M = 0.9$ and a Reynolds number of $Re_D = 2 \times 10^5$ have been simulated using a very fine grid of 3.1 billion points. They exit from a straight pipe nozzle with flow velocity conditions, including the momentum thickness and the shape factor of the boundary layer, the momentum-thickness-based Reynolds number, and the peak turbulence intensity, similar to those obtained in experiments for jets from the ASME and the conical nozzles. Thus, the nozzle-exit boundary layer is in a highly disturbed laminar state in the first case and in a turbulent state in the second case. The flow properties at the nozzle exit, in the shear layers, and on the jet centerline, as well as the far-field noise radiated by the two jets, have been investigated. The jet with the ASME-like initial conditions is found to contain more high-frequency velocity fluctuations at the nozzle exit than the other jet, which is most likely due to its thinner boundary layer. Its mixing layers also develop a little more rapidly, leading to a shorter potential core, with slightly higher turbulence intensities. The differences between the two cases are, however, small, and the flow and sound field of both jets are in good agreement with available experimental data for jets at $M = 0.9$ and $Re_D \geq 5 \times 10^5$. Finally, no extra noise components are noted for the

jet with the ASME-like exit flow conditions, contrary to what is observed in experiments with the ASME nozzle. Further experimental and numerical work is required to identify the reasons for this. In particular, additional measurements of the flow characteristics at the nozzle exit and in the shear layers for jets from the ASME nozzle would be very useful.

Appendix: Sensitivity to Near-Wall Mesh Spacing

To investigate the sensitivity of the LES results to the near-wall mesh spacing, a simulation of jetConic has been performed on a grid finer than the grid defined in Table 3. This new grid is limited to $z = 3.5r_0$ in the axial direction to save computational time. For $z \leq 3.5r_0$, it is identical to the other one in the directions θ and z but differs in the direction r , with a mesh spacing $\Delta r/r_0 = 0.08\%$ instead of $\Delta r/r_0 = 0.15\%$ at $r = r_0$. In the additional LES, the tripping procedure is exactly the same as in the LES using the first grid, and the time step is halved because of the CFL stability condition, leading to an application of the relaxation filtering that is twice as frequent. The flow properties obtained using the two grids at the nozzle exit and in the mixing layers are found to be very similar. Consequently, they depend neither on the wall-normal spacing nor on the explicit filtering applied to remove grid-to-grid oscillations as well as to relax subgrid-scale turbulent energy.

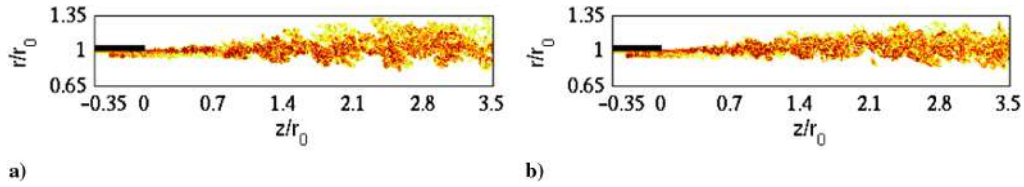


Fig. A1 Snapshots of vorticity norm obtained for jetConic using a) the grid defined in Table 3, and b) a finer grid with $\Delta r/r_0 = 0.08\%$ at $r = r_0$. The scale ranges up to the level of $40u_j/r_0$.

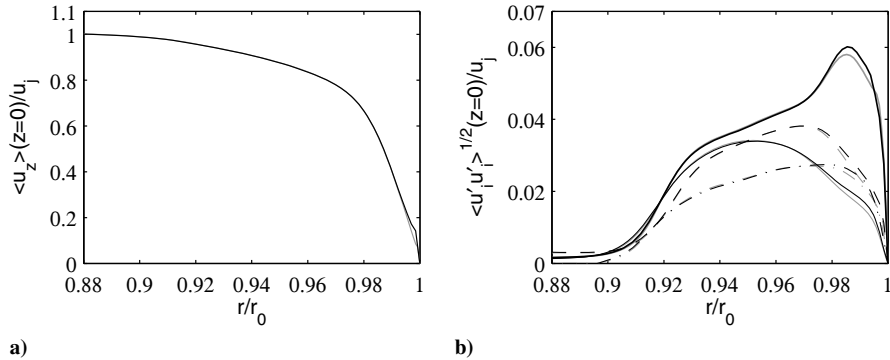


Fig. A2 Nozzle-exit profiles a) of $\langle u_z \rangle$, and b) of $\langle u'^2_z \rangle^{1/2}/u_j$ (thick line), $\langle u'^2_r \rangle^{1/2}/u_j$ (thin line), $\langle u'^2_\theta \rangle^{1/2}/u_j$ (dashed line), and $\langle u'_r u'_z \rangle^{1/2}/u_j$ (dash-dotted line) obtained for jetConic using (black) the reference grid and (gray) the finer grid.

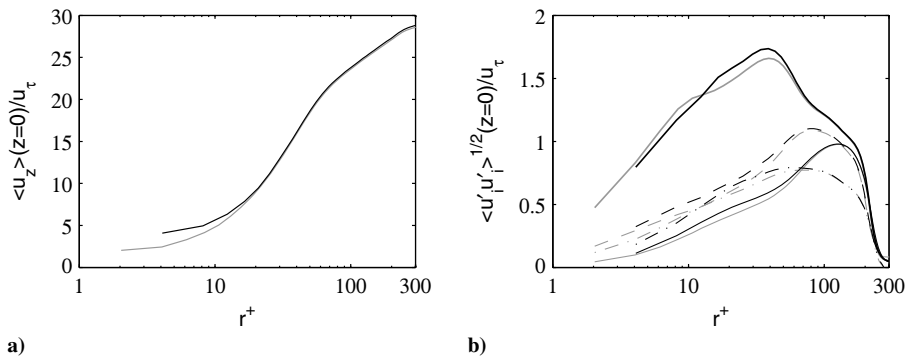


Fig. A3 Nozzle-exit profiles of a) mean axial velocity, and b) turbulence intensities, represented in wall units based on the wall friction velocity, same line types as in Fig. 19.

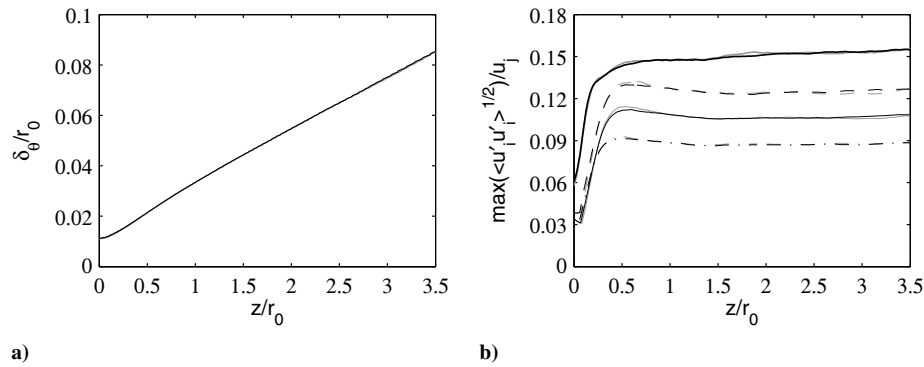


Fig. A4 Variations of a) momentum thickness, and b) the peak values of: $\langle u'u' \rangle^{1/2} / u_j$ (thick line), $\langle u'u' \rangle^{1/2} / u_j$ (thin line), $\langle u'u' \rangle^{1/2} / u_j$ (dashed line), and $\langle u'u' \rangle^{1/2} / u_j$ (dash-dotted line), obtained for jetConic using (black) the reference grid and (gray) the finer grid.

By way of illustration, some results are represented next, including vorticity snapshots in Figs. A1a and A1b, the radial profiles at the nozzle-exit of mean axial velocity and of turbulence intensities using outer units in Figs. A2a and A2b, and wall units in Figs. A3a and A3b as well as the variations of the shear-layer momentum thickness and of the peak turbulence intensities in Figs. A4a and A4b. In the last three figures, the solutions calculated with the reference grid (in black) and with the finer grid (in gray) superpose or are very close to each other.

Acknowledgments

This work was granted access to the High-Performance-Computing resources of Très Grand Centre de calcul of the Commissariat à l'Energie Atomique, of the Centre Informatique National de l'Enseignement Supérieur, and Institut du Développement et des Ressources en Informatique Scientifique under the allocation 2014-2a0204 made by Grand Equipement National de Calcul Intensif. It was performed within the framework of the Labex CeLyA of Université de Lyon, operated by the French National Research Agency (Grant No. ANR-10-LABX-0060/ANR-11-IDEX-0007).

References

- [1] Crow, S. C., and Champagne, F. H., "Orderly Structure in Jet Turbulence," *Journal of Fluid Mechanics*, Vol. 48, No. 3, 1971, pp. 547–591. doi:10.1017/S0022112071001745
- [2] Hill, W. G., Jenkins, R. C., and Gilbert, B. L., "Effects of the Initial Boundary-Layer State on Turbulent Jet Mixing," *AIAA Journal*, Vol. 14, No. 11, 1976, pp. 1513–1514. doi:10.2514/3.61491
- [3] Browand, F. K., and Latigo, B. O., "Growth of the Two-Dimensional Mixing Layer from a Turbulent and Nonturbulent Boundary Layer," *Physics of Fluids*, Vol. 22, No. 6, 1979, pp. 1011–1019. doi:10.1063/1.862705
- [4] Husain, Z. D., and Hussain, A. K. M. F., "Axisymmetric Mixing Layer: Influence of the Initial and Boundary Conditions," *AIAA Journal*, Vol. 17, No. 1, 1979, pp. 48–55. doi:10.2514/3.61061
- [5] Raman, G., Zaman, K. B. M. Q., and Rice, E. J., "Initial Turbulence Effect on Jet Evolution with and Without Tonal Excitation," *Physics of Fluids A*, Vol. 1, No. 7, 1989, pp. 1240–1248. doi:10.1063/1.857347
- [6] Raman, G., Rice, E. J., and Reshotko, E., "Mode Spectra of Natural Disturbances in a Circular Jet and the Effect of Acoustic Forcing," *Experiments in Fluids*, Vol. 17, No. 6, 1994, pp. 415–426. doi:10.1007/BF01877044
- [7] Zaman, K. B. M. Q., "Effect of Initial Condition on Subsonic Jet Noise," *AIAA Journal*, Vol. 23, No. 9, 1985, pp. 1370–1373. doi:10.2514/3.9094
- [8] Zaman, K. B. M. Q., "Far-Field Noise of a Subsonic Jet Under Controlled Excitation," *Journal of Fluid Mechanics*, Vol. 152, No. 1, 1985, pp. 83–111. doi:10.1017/S0022112085000581
- [9] Bridges, J. E., and Hussain, A. K. M. F., "Roles of Initial Conditions and Vortex Pairing in Jet Noise," *Journal of Sound and Vibration*, Vol. 117, No. 2, 1987, pp. 289–311. doi:10.1016/0022-460X(87)90540-2
- [10] Colonius, T., and Lele, S. K., "Computational Aeroacoustics: Progress on Nonlinear Problems of Sound Generation," *Progress in Aerospace Sciences*, Vol. 40, No. 6, 2004, pp. 345–416. doi:10.1016/j.paerosci.2004.09.001
- [11] Bailly, C., and Bogey, C., "Contributions of CAA to Jet Noise Research and Prediction," *International Journal of Computational Fluid Dynamics*, Vol. 18, No. 6, 2004, pp. 481–491. doi:10.1080/10618560410001673498
- [12] Wang, M., Freund, J. B., and Lele, S. K., "Computational Prediction of Flow-Generated Sound," *Annual Review of Fluid Mechanics*, Vol. 38, No. 1, 2006, pp. 483–512. doi:10.1146/annurev.fluid.38.050304.092036
- [13] Bodony, D. J., and Lele, S. K., "On the Current Status of Jet Noise Predictions Using Large-Eddy Simulation," *AIAA Journal*, Vol. 46, No. 2, 2008, pp. 364–380. doi:10.2514/1.24475
- [14] Boersma, B. J., Brethouwer, G., and Nieuwstadt, F. T. M., "A Numerical Investigation on the Effect of the Inflow Conditions on the Self-Similar Region of a Round Jet," *Physics of Fluids*, Vol. 10, No. 4, 1998, p. 899. doi:10.1063/1.869626
- [15] Stanley, S. A., and Sarkar, S., "Influence of Nozzle Conditions and Discrete Forcing on Turbulent Planar Jets," *AIAA Journal*, Vol. 38, No. 9, 2000, pp. 1615–1623. doi:10.2514/2.1144
- [16] Freund, J. B., "Noise Sources in a Low-Reynolds-Number Turbulent Jet at Mach 0.9," *Journal of Fluid Mechanics*, Vol. 438, July 2001, pp. 277–305. doi:10.1017/S0022112001004414
- [17] Zhao, W., Frankel, S. H., and Mongeau, L., "Large Eddy Simulations of Sound Radiation from Subsonic Turbulent Jets," *AIAA Journal*, Vol. 39, No. 8, 2001, pp. 1469–1477. doi:10.2514/2.1497
- [18] Bogey, C., Bailly, C., and Juvé, D., "Noise Investigation of a High Subsonic, Moderate Reynolds Number Jet Using a Compressible LES," *Theoretical and Computational Fluid Dynamics*, Vol. 16, No. 4, 2003, pp. 273–297. doi:10.1007/s00162-002-0079-4
- [19] Bodony, D. J., and Lele, S. K., "On Using Large-Eddy Simulation for the Prediction of Noise from Cold and Heated Turbulent Jets," *Physics of Fluids*, Vol. 17, No. 8, 2005, Paper 085103. doi:10.1063/1.2001689
- [20] Bogey, C., and Bailly, C., "Effects of Inflow Conditions and Forcing on a Mach 0.9 Jet and Its Radiated Noise," *AIAA Journal*, Vol. 43, No. 5, 2005, pp. 1000–1007. doi:10.2514/1.7465
- [21] Kim, J., and Choi, H., "Large Eddy Simulation of a Circular Jet: Effect of Inflow Conditions on the Near Field," *Journal of Fluid Mechanics*, Vol. 620, Feb. 2009, pp. 383–411. doi:10.1017/S0022112008004722
- [22] Shur, M. L., Spalart, P. R., and Strelets, M. K. H., "LES-Based Evaluation of a Microjet Noise Reduction Concept in Static and Flight Conditions," *Journal of Sound and Vibration*, Vol. 330, No. 17, 2011, pp. 4083–4097. doi:10.1016/j.jsv.2011.02.013
- [23] Andersson, N., Eriksson, L.-E., and Davidson, L., "Large-Eddy Simulation of Subsonic Turbulent Jets and Their Radiated Sound," *AIAA*

- Journal*, Vol. 43, No. 9, 2005, pp. 1899–1912.
doi:10.2514/1.13278
- [24] Bogey, C., and Bailly, C., “Influence of Nozzle-Exit Boundary-Layer Conditions on the Flow and Acoustic Fields of Initially Laminar Jets,” *Journal of Fluid Mechanics*, Vol. 663, Nov. 2010, pp. 507–538.
doi:10.1017/S0022112010003605
- [25] Bogey, C., Marsden, O., and Bailly, C., “Large-Eddy Simulation of the Flow and Acoustic Fields of a Reynolds Number 10^5 Subsonic Jet with Tripped Exit Boundary Layers,” *Physics of Fluids*, Vol. 23, No. 3, 2011, Paper 035104.
doi:10.1063/1.3555634
- [26] Bogey, C., Marsden, O., and Bailly, C., “On the Spectra of Nozzle-Exit Velocity Disturbances in Initially Nominally Turbulent Jets,” *Physics of Fluids*, Vol. 23, No. 9, 2011, Paper 091702.
doi:10.1063/1.3642642
- [27] Bogey, C., Marsden, O., and Bailly, C., “Influence of Initial Turbulence Level on the Flow and Sound Fields of a Subsonic Jet at a Diameter-Based Reynolds Number of 10^5 ,” *Journal of Fluid Mechanics*, Vol. 701, June 2012, pp. 352–385.
doi:10.1017/jfm.2012.162
- [28] Bogey, C., Marsden, O., and Bailly, C., “Effects of Moderate Reynolds Numbers on Subsonic Round Jets with Highly Disturbed Nozzle-Exit Boundary Layers,” *Physics of Fluids*, Vol. 24, No. 10, 2012, Paper 105107.
doi:10.1063/1.4757667
- [29] Bogey, C., and Marsden, O., “Identification of the Effects of the Nozzle-Exit Boundary-Layer Thickness and Its Corresponding Reynolds Number in Initially Highly Disturbed Subsonic Jets,” *Physics of Fluids*, Vol. 25, No. 5, 2013, Paper 055106.
doi:10.1063/1.4807071
- [30] Bogey, C., Barré, S., and Bailly, C., “Direct Computation of the Noise Generated by Subsonic Jets Originating from a Straight Pipe Nozzle,” *International Journal of Aeroacoustics*, Vol. 7, No. 1, 2008, pp. 1–21.
doi:10.1260/147547208784079917
- [31] Uzun, A., and Hussaini, M., “Investigation of High Frequency Noise Generation in the Near-Nozzle Region of a Jet Using Large Eddy Simulation,” *Theoretical and Computational Fluid Dynamics*, Vol. 21, No. 4, 2007, pp. 291–321.
doi:10.1007/s00162-007-0048-z
- [32] Sandberg, R. D., Sandham, N. D., and Saponitsky, V., “DNS of Compressible Pipe Flow Exiting Into a Coflow,” *International Journal of Heat and Fluid Flow*, Vol. 35, June 2012, pp. 33–44.
doi:10.1016/j.ijheatfluidflow.2012.01.006
- [33] Bühler, S., Kleiser, L., and Bogey, C., “Simulation of Subsonic Turbulent Nozzle-Jet Flow and Its Near-Field Sound,” *AIAA Journal*, Vol. 52, No. 8, 2014, pp. 1653–1669.
doi:10.2514/1.J052673
- [34] Bogey, C., and Marsden, O., “Influence of Nozzle-Exit Boundary-Layer Profile on High-Subsonic Jets,” *20th AIAA/CEAS Aeroacoustics Conference*, AIAA Paper 2014-2600, 2014.
- [35] Brès, G. A., Jaunet, V., Le Rallic, M., Jordan, P., Colonius, T., and Lele, S. K., “Large Eddy Simulation for Jet Noise: The Importance of Getting the Boundary Layer Right,” *21st AIAA/CEAS Aeroacoustics Conference*, AIAA Paper 2015-2535, 2015.
- [36] Le Bras, S., Deniau, H., Bogey, C., and Daviller, G., “Development of Compressible Large-Eddy Simulations Combining High-Order Schemes and Wall Modeling,” *21st AIAA/CEAS Aeroacoustics Conference*, AIAA Paper 2015-3135, 2015.
- [37] Viswanathan, K., “Aeroacoustics of Hot Jets,” *Journal of Fluid Mechanics*, Vol. 516, Oct. 2004, pp. 39–82.
doi:10.1017/S0022112004000151
- [38] Tanna, H. K., “An Experimental Study of Jet Noise. Part 1: Turbulent Mixing Noise,” *Journal of Sound and Vibration*, Vol. 50, No. 3, 1977, pp. 405–428.
doi:10.1016/0022-460X(77)90493-X
- [39] Harper-Bourne, M., “Jet Noise Measurements: Past and Present,” *International Journal of Aeroacoustics*, Vol. 9, Nos. 4–5, 2010, pp. 559–588.
- [40] Viswanathan, K., and Clark, L. T., “Effect of Nozzle Internal Contour on Jet Aeroacoustics,” *International Journal of Aeroacoustics*, Vol. 3, No. 2, 2004, pp. 103–135.
doi:10.1260/1475472041494819
- [41] Zaman, K. B. M. Q., “Effect of Initial Boundary-Layer State on Subsonic Jet Noise,” *AIAA Journal*, Vol. 50, No. 8, 2012, pp. 1784–1795.
doi:10.2514/1.J051712
- [42] Karon, A. Z., and Ahuja, K. K., “Effect of Nozzle-Exit Boundary Layer on Jet Noise,” *51st AIAA Aerospace Sciences Meeting*, AIAA Paper 2013-0615, Jan. 2013.
- [43] Fontaine, R. A., Elliott, G. S., Austin, J. M., and Freund, J. B., “Very Near-Nozzle Shear-Layer Turbulence and Jet Noise,” *Journal of Fluid Mechanics*, Vol. 770, May 2015, pp. 27–51.
doi:10.1017/jfm.2015.119
- [44] Schubauer, G. B., and Klebanoff, P. S., “Contributions on the Mechanics of Boundary-Layer Transition,” NACA TN-3498, 1955.
- [45] Klebanoff, P. S., and Diehl, Z.W., “Some Features of Artificially Thickened Fully Developed Turbulent Boundary Layers with Zero Pressure Gradient,” NACA TN-1110, 1952.
- [46] Coles, D. E., “The Turbulent Boundary Layer in a Compressible Fluid,” Rand Corp. Rept. R-403-PR, Santa Monica, CA, 1962.
- [47] Erm, P. L., and Joubert, P. N., “Low-Reynolds-Number Turbulent Boundary Layers,” *Journal of Fluid Mechanics*, Vol. 230, No. 1, 1991, pp. 1–44.
doi:10.1017/S0022112091000691
- [48] Schlatter, P., and Örlü, R., “Turbulent Boundary Layers at Moderate Reynolds Numbers: Inflow Length and Tripping Effects,” *Journal of Fluid Mechanics*, Vol. 710, Nov. 2012, pp. 5–34.
doi:10.1017/jfm.2012.324
- [49] Hutchings, N., “Caution: Tripping Hazards,” *Journal of Fluid Mechanics*, Vol. 710, Nov. 2012, pp. 1–4.
doi:10.1017/jfm.2012.419
- [50] Castillo, L., and Johansson, T. G., “The Effects of the Upstream Conditions on a Low Reynolds Number Turbulent Boundary Layer with Zero Pressure Gradient,” *Journal of Turbulence*, Vol. 3, 2002, p. 031.
doi:10.1088/1468-5248/3/1/031
- [51] Mohseni, K., and Colonius, T., “Numerical Treatment of Polar Coordinate Singularities,” *Journal of Computational Physics*, Vol. 157, No. 2, 2000, pp. 787–795.
doi:10.1006/jcph.1999.6382
- [52] Bogey, C., de Cacqueray, N., and Bailly, C., “Finite Differences for Coarse Azimuthal Discretization and for Reduction of Effective Resolution near Origin of Cylindrical Flow Equations,” *Journal of Computational Physics*, Vol. 230, No. 4, 2011, pp. 1134–1146.
doi:10.1016/j.jcp.2010.10.031
- [53] Bogey, C., and Bailly, C., “A Family of Low Dispersive and Low Dissipative Explicit Schemes for Flow and Noise Computations,” *Journal of Computational Physics*, Vol. 194, No. 1, 2004, pp. 194–214.
doi:10.1016/j.jcp.2003.09.003
- [54] Bogey, C., de Cacqueray, N., and Bailly, C., “A Shock-Capturing Methodology Based on Adaptive Spatial Filtering for High-Order Non-Linear Computations,” *Journal of Computational Physics*, Vol. 228, No. 5, 2009, pp. 1447–1465.
doi:10.1016/j.jcp.2008.10.042
- [55] Berland, J., Bogey, C., Marsden, O., and Bailly, C., “High-Order, Low Dispersive and Low Dissipative Explicit Schemes for Multi-Scale and Boundary Problems,” *Journal of Computational Physics*, Vol. 224, No. 2, 2007, pp. 637–662.
doi:10.1016/j.jcp.2006.10.017
- [56] Tam, C. K. W., and Dong, Z., “Radiation and Outflow Boundary Conditions for Direct Computation of Acoustic and Flow Disturbances in a Nonuniform Mean Flow,” *Journal of Computational Acoustics*, Vol. 4, No. 2, 1996, pp. 175–201.
doi:10.1142/S0218396X96000040
- [57] Bogey, C., and Bailly, C., “Three-Dimensional Non Reflective Boundary Conditions for Acoustic Simulations: Far-Field Formulation and Validation Test Cases,” *Acta Acustica*, Vol. 88, No. 4, 2002, pp. 463–471.
- [58] Bogey, C., and Bailly, C., “Large Eddy Simulations of Transitional Round Jets: Influence of the Reynolds Number on Flow Development and Energy Dissipation,” *Physics of Fluids*, Vol. 18, No. 6, 2006, Paper 065101.
doi:10.1063/1.2204060
- [59] Bogey, C., and Bailly, C., “Turbulence and Energy Budget in a Self-Preserving Round Jet: Direct Evaluation Using Large-Eddy Simulation,” *Journal of Fluid Mechanics*, Vol. 627, May 2009, pp. 129–160.
doi:10.1017/S0022112009005801
- [60] Fauconnier, D., Bogey, C., and Dick, E., “On the Performance of Relaxation Filtering for Large-Eddy Simulation,” *Journal of Turbulence*, Vol. 14, No. 1, 2013, pp. 22–49.
doi:10.1080/14685248.2012.740567
- [61] Kremer, F., and Bogey, C., “Large-Eddy Simulation of Turbulent Channel Flow Using Relaxation Filtering: Resolution Requirement and Reynolds Number Effects,” *Computers & Fluids*, Vol. 116, Aug. 2015, pp. 17–28.
doi:10.1016/j.compfluid.2015.03.026
- [62] Kim, J., Moin, P., and Moser, R., “Turbulence Statistics in Fully Developed Channel Flow at Low Reynolds Number,” *Journal of Fluid Mechanics*, Vol. 177, No. 1, 1987, pp. 133–166.
doi:10.1017/S0022112087000892

- [63] Spalart, P. R., "Direct Simulation of a Turbulent Boundary Layer up to $R_\theta = 1410$," *Journal of Fluid Mechanics*, Vol. 187, No. 1, 1988, pp. 61–98.
doi:10.1017/S0022112088000345
- [64] Gloerfelt, X., and Berland, J., "Turbulent Boundary Layer Noise: Direct Radiation at Mach Number 0.5," *Journal of Fluid Mechanics*, Vol. 723, May 2013, pp. 318–351.
doi:10.1017/jfm.2013.134
- [65] Bogey, C., Barré, S., Juvé, D., and Bailly, C., "Simulation of a Hot Coaxial Jet: Direct Noise Prediction and Flow-Acoustics Correlations," *Physics of Fluids*, Vol. 21, No. 3, 2009, Paper 035105.
doi:10.1063/1.3081561
- [66] Ahuja, K. K., Tester, B. J., and Tanna, H. K., "Calculation of Far Field Jet Noise Spectra from Near Field Measurements with True Source Location," *Journal of Sound and Vibration*, Vol. 116, No. 3, 1987, pp. 415–426.
doi:10.1016/S0022-460X(87)81374-3
- [67] Viswanathan, K., "Distributions of Noise Sources in Heated and Cold Jets: Are They Different?" *International Journal of Aeroacoustics*, Vol. 9, Nos. 4–5, 2006, pp. 589–626.
- [68] Brown, G. L., and Roshko, A., "On Density Effects and Large Structure in Turbulent Mixing Layers," *Journal of Fluid Mechanics*, Vol. 64, No. 4, 1974, pp. 775–816.
doi:10.1017/S002211207400190X
- [69] Arndt, R. E. A., Long, D. F., and Glauser, M. N., "The Proper Orthogonal Decomposition of Pressure Fluctuations Surrounding a Turbulent Jet," *Journal of Fluid Mechanics*, Vol. 340, June 1997, pp. 1–33.
doi:10.1017/S0022112097005089
- [70] Coiffet, F., Jordan, P., Delville, J., Gervais, Y., and Ricaud, F., "Coherent Structures in Subsonic Jets: A Quasi-Irrotational Source Mechanism?" *International Journal of Aeroacoustics*, Vol. 5, No. 1, 2005, pp. 67–89.
doi:10.1260/147547206775220407
- [71] Mollo-Christensen, E., Kolpin, M. A., and Martuccelli, J. R., "Experiments on Jet Flows and Jet Noise Far-Field Spectra and Directivity Patterns," *Journal of Fluid Mechanics*, Vol. 18, No. 2, 1964, pp. 285–301.
doi:10.1017/S0022112064000209
- [72] Lush, P. A., "Measurements of Subsonic Jet Noise and Comparison with Theory," *Journal of Fluid Mechanics*, Vol. 46, No. 3, 1971, pp. 477–500.
doi:10.1017/S002211207100065X
- [73] Tam, C. K. W., Viswanathan, K., Ahuja, K. K., and Panda, J., "The Sources of Jet Noise: Experimental Evidence," *Journal of Fluid Mechanics*, Vol. 615, Nov. 2008, pp. 253–292.
doi:10.1017/S0022112008003704
- [74] Fernholz, H. H., and Finley, P. J., "The Incompressible Zero-Pressure-Gradient Turbulent Boundary Layer: An Assessment of the Data," *Progress in Aerospace Sciences*, Vol. 32, No. 4, 1996, pp. 245–311.
doi:10.1016/0376-0421(95)00007-0
- [75] Tomkins, C. D., and Adrian, R. J., "Energetic Spanwise Modes in the Logarithmic Layer of a Turbulent Boundary Layer," *Journal of Fluid Mechanics*, Vol. 545, No. 1, 2005, pp. 141–162.
doi:10.1017/S0022112005006397
- [76] Fleury, V., Bailly, C., Jondeau, E., Michard, M., and Juvé, D., "Space-Time Correlations in Two Subsonic Jets Using Dual-PIV Measurements," *AIAA Journal*, Vol. 46, No. 10, 2008, pp. 2498–2509.
doi:10.2514/1.35561
- [77] Castelain, T., "Contrôle de Jet par Microjets Impactants. Mesure de Bruit Rayonné et Analyse Aérodynamique," Ph.D. Thesis, École Centrale de Lyon, Lyon, France, 2006.
- [78] Fleury, V., "Superdirectivité, Bruit d'Appariement et Autres Contributions au Bruit de Jet Subsonique," Ph.D. Thesis, École Centrale de Lyon, Lyon, France, 2006.
- [79] Bridges, J., and Wernet, M. P., "Validating Large-Eddy Simulation for Jet Aeroacoustics," *Journal of Propulsion and Power*, Vol. 28, No. 2, 2012, pp. 226–235.
doi:10.2514/1.B34385
- [80] Michalke, A., "Survey on Jet Instability Theory," *Progress in Aerospace Sciences*, Vol. 21, 1984, pp. 159–199.
doi:10.1016/0376-0421(84)90005-8
- [81] Gutmark, E., and Ho, C.-M., "Preferred Modes and the Spreading Rates of Jets," *Physics of Fluids*, Vol. 26, No. 10, 1983, pp. 2932–2938.
doi:10.1063/1.864058
- [82] Bridges, J., "Effect of Heat on Space-Time Correlations in Jets," *12th AIAA/CEAS Aeroacoustics Conference*, AIAA Paper 2006-2534, May 2006.
- [83] Lau, J. C., Morris, P. J., and Fisher, M. J., "Measurements in Subsonic and Supersonic Free Jets Using a Laser Velocimeter," *Journal of Fluid Mechanics*, Vol. 93, No. 1, 1979, pp. 1–27.
doi:10.1017/S0022112079001750
- [84] Arakeri, V. H., Krothapalli, A., Siddavaram, V., Alkislal, M. B., and Lourenco, L., "On the Use of Microjets to Suppress Turbulence in a Mach 0.9 Axisymmetric Jet," *Journal of Fluid Mechanics*, Vol. 490, Sept. 2003, pp. 75–98.
doi:10.1017/S0022112003005202
- [85] Bridges, J., and Wernet, M. P., "Effect of Temperature on Jet Velocity Spectra," *13th AIAA/CEAS Aeroacoustics Conference*, AIAA Paper 2007-3628, 2007.
- [86] Bridges, J., and Brown, C. A., "Validation of the Small Hot Jet Acoustic Rig for Aeroacoustics," *11th AIAA/CEAS Aeroacoustics Conference*, AIAA Paper 2005-2846, May 2005.
- [87] Brown, C., and Bridges, J., "Small Hot Jet Acoustic Rig Validation," NASA TM-2006-214234, 2006.